Measurements of the Elliptic and Triangular Azimuthal Anisotropies in Central ^{3}He + Au, d + Au and p + Au Collisions at $\sqrt{s_{NN}} = 200$ GeV

M. I. Abdulhamid,[4] B. E. Aboona,[54] J. Adam,[15] J. R. Adams,[39] G. Agakishiev,[29] I. Aggarwal,[40] M. M. Aggarwal,[40] Z. Ahammed,[60] A. Aitbaev,[29] I. Alekseev,[2,36] D. M. Anderson,[54] A. Aparin,[29] S. Aslam,[25] J. Atchison,[1] G. S. Averichev,[29] V. Bairathi,[52] W. Baker,[11] J. G. Ball Cap,[21] K. Barish,[11] P. Bhagat,[28] A. Bhasin,[28] S. Bhatta,[51] I. G. Bordyuzhin,[2] J. D. Brandenburg,[39] A. V. Brandin,[36] X. Z. Cai,[49] H. Caines,[62] M. Calderón de la Barca Sánchez,[9] D. Cebra,[9] J. Ceska,[15] I. Chakaberia,[32] B. K. Chan,[10] Z. Chang,[26] A. Chatterjee,[16] D. Chen,[11] J. Chen,[48] J. H. Chen,[19] Z. Chen,[48] J. Cheng,[56] Y. Cheng,[10] S. Choudhury,[19] W. Christie,[6] X. Chu,[6] H. J. Crawford,[8] G. Dale-Gau,[13] A. Das,[15] M. Daugherity,[1] T. G. Dedovich,[29] I. M. Deppner,[20] A. A. Derevschikov,[41] A. Dhamija,[40] L. Di Carlo,[61] L. Didenko,[6] P. Dixit,[23] X. Dong,[32] J. L. Drachenberg,[1] E. Duckworth,[30] J. C. Dunlop,[6] J. Engelage,[8] G. Eppley,[43] S. Esumi,[57] O. Evdokimov,[13] A. Ewigleben,[33] O. Eyser,[6] R. Fatemi,[31] S. Fazio,[7] C. J. Feng,[38] Y. Feng,[42] E. Finch,[50] Y. Fisyak,[6] F. A. Flor,[62] C. Fu,[12] F. Geurts,[43] N. Ghimire,[53] A. Gibson,[59] K. Gopal,[24] X. Gou,[48] D. Grosnick,[59] A. Gupta,[28] A. Hamed,[4] Y. Han,[43] M. D. Harasty,[9] J. W. Harris,[62] H. Harrison-Smith,[31] W. He,[19] X. H. He,[27] Y. He,[48] C. Hu,[27] Q. Hu,[27] Y. Hu,[32] H. Huang,[38] H. Z. Huang,[10] S. L. Huang,[51] T. Huang,[13] X. Huang,[56] Y. Huang,[56] Y. Huang,[12] T. J. Humanic,[39] D. Isenhower,[1] M. Isshiki,[57] W. W. Jacobs,[26] A. Jalotra,[28] C. Jena,[24] Y. Ji,[32] J. Jia,[6,51] C. Jin,[43] X. Ju,[45] E. G. Judd,[8] S. Kabana,[52] M. L. Kabir,[11] D. Kalinkin,[31] K. Kang,[56] D. Kapukchyan,[11] K. Kauder,[6] H. W. Ke,[6] D. Keane,[30] A. Kechechyan,[29] M. Kelsey,[61] B. Kimelman,[9] A. Kiselev,[6] A. G. Knospe,[33] H. S. Ko,[32] L. Kochenda,[36] A. A. Korobitsin,[29] P. Kravtsov,[36] L. Kumar,[40] S. Kumar,[27] R. Kunnawalkam Elayavalli,[62] R. Lacey,[51] J. M. Landgraf,[6] A. Lebedev,[6] R. Lednicky,[29] J. H. Lee,[6] Y. H. Leung,[20] N. Lewis,[6] C. Li,[48] W. Li,[43] X. Li,[45] Y. Li,[45] Y. Li,[56] Z. Li,[45] X. Liang,[11] Y. Liang,[30] T. Lin,[48] C. Liu,[27] F. Liu,[12] G. Liu,[46] H. Liu,[26] H. Liu,[12] L. Liu,[12] T. Liu,[62] X. Liu,[39] Y. Liu,[54] Z. Liu,[12] T. Ljubicic,[6] W. J. Llope,[61] O. Lomicky,[15] R. S. Longacre,[6] E. M. Loyd,[11] T. Lu,[27] N. S. Lukow,[53] X. F. Luo,[12] V. B. Luong,[29] L. Ma,[19] R. Ma,[6] Y. G. Ma,[19] N. Magdy,[51] D. Mallick,[37] S. Margetis,[30] H. S. Matis,[32] J. A. Mazer,[44] G. McNamara,[61] K. Mi,[12] N. G. Minaev,[41] B. Mohanty,[37] M. M. Mondal,[37] I. Mooney,[62] D. A. Morozov,[41] A. Mudrokh,[29] M. I. Nagy,[17] A. S. Nain,[40] J. D. Nam,[53] Md. Nasim,[23] D. Neff,[10] J. M. Nelson,[8] D. B. Nemes,[62] M. Nie,[48] G. Nigmatkulov,[36] T. Niida,[57] R. Nishitani,[57] L. V. Nogach,[41] T. Nonaka,[57] G. Odyniec,[32] A. Ogawa,[6] S. Oh,[47] V. A. Okorokov,[36] K. Okubo,[57] B. S. Page,[6] R. Pak,[6] J. Pan,[54] A. Pandav,[37] A. K. Pandey,[27] Y. Panebratsev,[29] T. Pani,[44] P. Parfenov,[36] A. Paul,[11] C. Perkins,[8] B. R. Pokhrel,[53] M. Posik,[53] T. Protzman,[33] N. K. Pruthi,[40] J. Putschke,[61] Z. Qin,[56] H. Qiu,[27] A. Quintero,[53] C. Racz,[11] S. K. Radhakrishnan,[30] N. Raha,[61] R. L. Ray,[55] H. G. Ritter,[32] C. W. Robertson,[42] O. V. Rogachevsky,[29] M. A. Rosales Aguilar,[31] D. Roy,[44] L. Ruan,[6] A. K. Sahoo,[23] N. R. Sahoo,[48] H. Sako,[57] S. Salur,[44] E. Samigullin,[2] S. Sato,[57] W. B. Schmidke,[6] N. Schmitz,[34] J. Seger,[14] R. Seto,[11] P. Seyboth,[34] N. Shah,[25] E. Shahaliev,[29] P. V. Shanmuganathan,[6] T. Shao,[19] M. Sharma,[28] N. Sharma,[23] R. Sharma,[24] S. R. Sharma,[24] A. I. Sheikh,[30] D. Y. Shen,[19] K. Shen,[45] S. S. Shi,[12] Y. Shi,[48] Q. Y. Shou,[19] F. Si,[45] J. Singh,[40] S. Singha,[27] P. Sinha,[24] M. J. Skoby,[5,42] Y. Söhngen,[20] Y. Song,[62] B. Srivastava,[42] T. D. S. Stanislaus,[59] D. J. Stewart,[61] M. Strikhanov,[36] B. Stringfellow,[42] Y. Su,[45] C. Sun,[51] X. Sun,[27] Y. Sun,[45] Y. Sun,[22] B. Surrow,[53] D. N. Svirida,[2] Z. W. Sweger,[9] A. Tamis,[62] A. H. Tang,[6] Z. Tang,[45] A. Taranenko,[36] T. Tarnowsky,[35] J. H. Thomas,[32] D. Tlusty,[14] T. Todoroki,[57] M. V. Tokarev,[29] C. A. Tomkiel,[33] S. Trentalange,[10] R. E. Tribble,[54] P. Tribedy,[6] O. D. Tsai,[10,6] C. Y. Tsang,[30,6] Z. Tu,[6] T. Ullrich,[6] D. G. Underwood,[3,59] I. Upsal,[43] G. Van Buren,[6] A. N. Vasiliev,[41,36] V. Verkest,[61] F. Videbæk,[6] S. Vokal,[29] S. A. Voloshin,[61] F. Wang,[42] G. Wang,[10] J. S. Wang,[22] X. Wang,[48] Y. Wang,[45] Y. Wang,[12] Y. Wang,[56] Z. Wang,[48] J. C. Webb,[6] P. C. Weidenkaff,[20] G. D. Westfall,[35] H. Wieman,[32] G. Wilks,[13] S. W. Wissink,[26] J. Wu,[12] J. Wu,[27] X. Wu,[10] Y. Wu,[11] B. Xi,[49] Z. G. Xiao,[56] G. Xie,[58] W. Xie,[42] H. Xu,[22] N. Xu,[32] Q. H. Xu,[48] Y. Xu,[48] Y. Xu,[12] Z. Xu,[6] Z. Xu,[10] G. Yan,[48] Z. Yan,[51] C. Yang,[48] Q. Yang,[48] S. Yang,[46] Y. Yang,[38] Z. Ye,[43] Z. Ye,[13] L. Yi,[48] K. Yip,[6] Y. Yu,[48] W. Zha,[45] C. Zhang,[51] D. Zhang,[12] J. Zhang,[48] S. Zhang,[45] W. Zhang,[46] X. Zhang,[27] Y. Zhang,[27] Y. Zhang,[45] Y. Zhang,[12] Z. J. Zhang,[38] Z. Zhang,[6] Z. Zhang,[13] F. Zhao,[27] J. Zhao,[19] M. Zhao,[6] C. Zhou,[19] J. Zhou,[45] S. Zhou,[12] Y. Zhou,[12] X. Zhu,[56] M. Zurek,[3,6] and M. Zyzak[18]

(STAR Collaboration)

[1]*Abilene Christian University, Abilene, Texas 79699*
[2]*Alikhanov Institute for Theoretical and Experimental Physics NRC "Kurchatov Institute", Moscow 117218*
[3]*Argonne National Laboratory, Argonne, Illinois 60439*
[4]*American University of Cairo, New Cairo 11835, New Cairo, Egypt*

[5]*Ball State University, Muncie, Indiana, 47306*
[6]*Brookhaven National Laboratory, Upton, New York 11973*
[7]*University of Calabria & INFN-Cosenza, Rende 87036, Italy*
[8]*University of California, Berkeley, California 94720*
[9]*University of California, Davis, California 95616*
[10]*University of California, Los Angeles, California 90095*
[11]*University of California, Riverside, California 92521*
[12]*Central China Normal University, Wuhan, Hubei 430079*
[13]*University of Illinois at Chicago, Chicago, Illinois 60607*
[14]*Creighton University, Omaha, Nebraska 68178*
[15]*Czech Technical University in Prague, FNSPE, Prague 115 19, Czech Republic*
[16]*National Institute of Technology Durgapur, Durgapur - 713209, India*
[17]*ELTE Eötvös Loránd University, Budapest, Hungary H-1117*
[18]*Frankfurt Institute for Advanced Studies FIAS, Frankfurt 60438, Germany*
[19]*Fudan University, Shanghai, 200433*
[20]*University of Heidelberg, Heidelberg 69120, Germany*
[21]*University of Houston, Houston, Texas 77204*
[22]*Huzhou University, Huzhou, Zhejiang 313000*
[23]*Indian Institute of Science Education and Research (IISER), Berhampur 760010, India*
[24]*Indian Institute of Science Education and Research (IISER) Tirupati, Tirupati 517507, India*
[25]*Indian Institute Technology, Patna, Bihar 801106, India*
[26]*Indiana University, Bloomington, Indiana 47408*
[27]*Institute of Modern Physics, Chinese Academy of Sciences, Lanzhou, Gansu 730000*
[28]*University of Jammu, Jammu 180001, India*
[29]*Joint Institute for Nuclear Research, Dubna 141 980*
[30]*Kent State University, Kent, Ohio 44242*
[31]*University of Kentucky, Lexington, Kentucky 40506-0055*
[32]*Lawrence Berkeley National Laboratory, Berkeley, California 94720*
[33]*Lehigh University, Bethlehem, Pennsylvania 18015*
[34]*Max-Planck-Institut für Physik, Munich 80805, Germany*
[35]*Michigan State University, East Lansing, Michigan 48824*
[36]*National Research Nuclear University MEPhI, Moscow 115409*
[37]*National Institute of Science Education and Research, HBNI, Jatni 752050, India*
[38]*National Cheng Kung University, Tainan 70101*
[39]*The Ohio State University, Columbus, Ohio 43210*
[40]*Panjab University, Chandigarh 160014, India*
[41]*NRC "Kurchatov Institute", Institute of High Energy Physics, Protvino 142281*
[42]*Purdue University, West Lafayette, Indiana 47907*
[43]*Rice University, Houston, Texas 77251*
[44]*Rutgers University, Piscataway, New Jersey 08854*
[45]*University of Science and Technology of China, Hefei, Anhui 230026*
[46]*South China Normal University, Guangzhou, Guangdong 510631*
[47]*Sejong University, Seoul, 05006, South Korea*
[48]*Shandong University, Qingdao, Shandong 266237*
[49]*Shanghai Institute of Applied Physics, Chinese Academy of Sciences, Shanghai 201800*
[50]*Southern Connecticut State University, New Haven, Connecticut 06515*
[51]*State University of New York, Stony Brook, New York 11794*
[52]*Instituto de Alta Investigación, Universidad de Tarapacá, Arica 1000000, Chile*
[53]*Temple University, Philadelphia, Pennsylvania 19122*
[54]*Texas A&M University, College Station, Texas 77843*
[55]*University of Texas, Austin, Texas 78712*
[56]*Tsinghua University, Beijing 100084*
[57]*University of Tsukuba, Tsukuba, Ibaraki 305-8571, Japan*
[58]*University of Chinese Academy of Sciences, Beijing, 101408*
[59]*Valparaiso University, Valparaiso, Indiana 46383*
[60]*Variable Energy Cyclotron Centre, Kolkata 700064, India*
[61]*Wayne State University, Detroit, Michigan 48201*
[62]*Yale University, New Haven, Connecticut 06520*

The elliptic (v_2) and triangular (v_3) azimuthal anisotropy coefficients in central ^{3}He + Au, d + Au, and p + Au collisions at $\sqrt{s_{NN}} = 200$ GeV are measured as a function of transverse momentum (p_T) at midrapidity ($|\eta| < 0.9$), via the azimuthal angular correlation between two particles both at $|\eta| < 0.9$. While the $v_2(p_T)$ values depend on the colliding systems, the $v_3(p_T)$ values are system independent within the uncertainties, suggesting an influence on eccentricity from subnucleonic fluctuations in these small-sized systems. These results also provide stringent constraints for the hydrodynamic modeling of these systems.

Relativistic heavy-ion collisions produce the Quark Gluon Plasma (QGP), which has an anisotropic transverse energy density profile [1–5]. The eccentricity of this density profile can induce anisotropic pressure gradients, giving rise to strong anisotropies of particle distribution relative to the flow planes Ψ_n [6–8]. This anisotropy is often quantified via Fourier decomposition of the two-particle correlations in the relative azimuthal angle $\Delta\phi = \phi_\alpha - \phi_\beta$ [7,9] for the particles α and β as a function of the transverse momentum (p_T):

$$\frac{dN^{\text{pairs}}}{d\Delta\phi} \propto 1 + 2\sum_{n=1}^{\infty} c_n \cos(n\Delta\phi),$$

$$c_n(p_T^\alpha, p_T^\beta) = v_n(p_T^\alpha)v_n(p_T^\beta) + \delta_{\text{NF}}, \qquad (1)$$

where δ_{NF} represents the correlation unrelated to collective effects ("nonflow" correlation). The $v_2\{2\}$ and $v_3\{2\}$ (termed v_2 and v_3) harmonics that are linearly related to the respective eccentricities of initial energy density spatial distribution, $\varepsilon_2\{2\}$ and $\varepsilon_3\{2\}$, provide an important model constraint on the specific shear viscosity of the QGP produced in large- to moderate-sized A + A systems such as Pb + Pb, Au + Au and Cu + Cu collisions [8,10–18].

For small-sized systems such as $p + p$, $p/d/^3$He + A collisions, the azimuthal anisotropies have been extensively measured at RHIC [19–25] and the LHC [26–29]. Numerical simulations suggest that hydrodynamics remains applicable even when the system size is of the order of the inverse temperature [30]. However, the influence of subnucleonic fluctuations on the initial geometry, which is negligible for larger-sized systems, has not been charted for small-sized systems. Such fluctuations can result from a spatially inhomogeneous gluon field distribution inside the nucleon [31,32].

Table I gives an illustrative comparison of the eccentricities for ^{3}He + Au, d + Au, and p + Au collisions from four scenarios, all based on Glauber models and labeled as a, b, c, and d. Model a corresponds to the mean eccentricities reported in Ref. [33]; it uses the default Glauber model to calculate the nucleon position and does not have quantum fluctuations. Model b also uses the default Glauber for nucleon position but includes quantum fluctuations characterized by a smoothly distributed Gaussian-like gluon field inside each nucleon [31].

In Models c and d, there are several gluon fields surrounding the valence quarks inside the nucleon instead of one gluon field as in Model b. The distribution of the gluon field is Gaussian-like in Model c [31] but is lumpy for the IP-Glasma framework [22,32] used in Model d. Table I shows that the system dependence of $\varepsilon_{2,3}$ is strongly influenced by subnucleonic fluctuations, suggesting that measurements of the system dependence of $v_{2,3}(p_T)$ can provide invaluable constraints on the role of such fluctuations in small-sized systems and give insights into the structure of the nucleon.

Furthermore, the anisotropy may also originate from nonhydrodynamic modes [35–41] and/or large hydrodynamic gradient-expansion corrections [42,43] due to the short lifetime of the created medium. Therefore, whether hydrodynamics can extend its success from large- and moderate-sized systems to small-sized systems remains uncertain.

Prior measurements of $v_{2,3}(p_T)$ for ^{3}He + Au, d + Au, and p + Au collisions have been reported by the PHENIX Collaboration [21–23]. These measurements, which utilized correlations between particles at the middle and backward pseudorapidity (η), indicated values compatible with the system dependence of ε_n^a and little influence from subnucleonic fluctuations. Here, we present complementary v_n measurements for pseudorapidity $|\eta| < 0.9$ via correlations between particles both at middle

TABLE I. Comparison of the system dependence of $\varepsilon_2(\varepsilon_3)$ in central ^{3}He + Au, d + Au, and p + Au collisions from four Glauber-based models (see text). For Model a and d, the $\langle\varepsilon_2\rangle$ and $\langle\varepsilon_3\rangle$ values are obtained for impact parameter b < 2 fm; for Models b and c, the ε_n values are obtained as $\sqrt{\langle\varepsilon_n^2\rangle}$ for 0–10% ^{3}He + Au and d + Au, and 0–2% p + Au collisions selected by multiplicity. The relative difference of the ε_n values for the three systems is not strongly influenced by the difference in event selection nor the ε_n definition. The statistical uncertainties are much less than 1%.

Model	a [33,34] $\varepsilon_2^a(\varepsilon_3^a)$	b [31] $\varepsilon_2^b(\varepsilon_3^b)$	c [31] $\varepsilon_2^c(\varepsilon_3^c)$	d [22,32] $\varepsilon_2^d(\varepsilon_3^d)$
^{3}He + Au	0.50(0.28)	0.52(0.35)	0.53(0.38)	0.64(0.46)
d + Au	0.54(0.18)	0.51(0.32)	0.53(0.36)	0.73(0.40)
p + Au	0.23(0.16)	0.34(0.27)	0.41(0.34)	0.50(0.32)

pseudorapidity to investigate further a possible role for subnucleonic fluctuations. The two-particle azimuthal correlations employed for the measurements suppress the influence of nonflow correlations via the requirement $|\Delta\eta| > 1.0$ in conjunction with three established methods of nonflow subtraction [44–50].

The ^{3}He + Au, d + Au, p + Au, and p + p data used in this analysis are collected with minimum bias (MB) and high multiplicity (HM) triggers in 2014, 2015, and 2016 experimental runs of the STAR experiment at $\sqrt{s_{NN}} = 200$ GeV. Events were selected to be within a radius $r < 2$ cm relative to the beam axis and within specific ranges of the center of the time projection chamber (TPC) in the direction along the beam axis v_z with the values ± 30 cm for ^{3}He + Au, ± 15 cm for d + Au, ± 20 cm for p + Au, and ± 20 cm for p + p. The MB trigger for p + p, p + Au, d + Au collisions required a coincidence between both sides of the vertex position detectors (VPD) [51] along the beam pipe, which span the range $4.4 < |\eta| < 4.9$. The MB trigger for ^{3}He + Au employed a coincidence between both sides of the VPD, a coincidence between both sides of the beam-beam counters (BBC) [52] which span the range $3.3 < |\eta| < 5.1$, and a neutron hit in the zero degree calorimeter (ZDC) [53] on the Au-going side. For p + Au collisions, the MB triggers were augmented with a number-of-hits cut of more than 80 in the barrel time of flight (BTOF) detector with $|\eta| < 1$ [54] to obtain the HM triggers.

The collision centrality is determined via Monte Carlo Glauber model calculations [55,56] tuned to match the distribution of the number of reconstructed charged tracks before efficiency correction ($N_{\rm ch}^{\rm off}$) in the MB events. To count $N_{\rm ch}^{\rm off}$, tracks are selected to have $|\eta| < 0.9$ and $0.2 < p_T < 3.0$ GeV/c with a matched hit in the BTOF detector. In this work, we use the top 0–10% centrality for d + Au, and both 0–10% and 10–20% for ^{3}He + Au collisions. For p + Au collisions, the HM datasets, supplemented with a threshold cut on $N_{\rm ch}^{\rm off}$, are used to select ultracentral (UC) events. This choice facilitates the comparison of the v_n measurements for UC p + Au, 0–10% d + Au, and 10–20% ^{3}He + Au with comparable track multiplicity after efficiency correction ($\langle N_{\rm ch}\rangle$), as listed in Table II. Note that $\langle N_{\rm ch}\rangle$ for the UC p + Au is also similar to that for the 0–2% p + Au MB data sample. The charged-hadron efficiency is obtained via the embedding of simulated charged pions [57,58] into actual data. The systematic uncertainties for $\langle N_{\rm ch}\rangle$ listed in Table II arise mainly from the uncertainties of $\pi^\pm$ reconstruction efficiency. There are additional 10% overall systematic uncertainties that arise from the efficiency estimations, which combine $\pi^\pm$, $K^\pm$, and (anti-)protons together. And such uncertainties are largely canceled out in flow measurements.

The charged particles detected in the TPC [59] are used to construct two-particle yield distributions $Y(\Delta\phi) = 1/N_{\rm Trig} dN/d\Delta\phi$ with efficiency correction applied. The

TABLE II. The average of efficiency-corrected multiplicity, $\langle N_{\rm ch}\rangle$, in MB p + p and central $p/d/^3$He + Au collisions at $\sqrt{s_{NN}} = 200$ GeV. The uncertainties reflect both systematic and statistical uncertainties.

	MB	UC	0–10%	10–20%	0–10%
	p + p	p + Au	d + Au	^{3}He + Au	^{3}He + Au
$\langle N_{\rm ch}\rangle$	4.7 ± 0.3	34.1 ± 1.7	35.6 ± 1.8	33.1 ± 1.7	47.7 ± 2.4

detector acceptance effects have been corrected by pairs from different events. The effect of multiple collisions from a bunch crossing (pileup) is primarily suppressed by requiring a matched hit in the BTOF detector or one of the two layers of silicon strip sensors of the heavy flavor tracker (HFT) detector [60], both of which have fast responses.

Figures 1(a)–1(d) show the distributions $Y(\Delta\phi)$ for central ^{3}He + Au, d + Au, p + Au, and MB p + p collisions as a function of $\Delta\phi$. The trigger (Trig.) and the associated (Assoc.) particles are measured in the range $0.2 < p_T < 2.0$ GeV/c and $1.0 < |\Delta\eta| < 1.8$. The near-($|\Delta\phi| < 1.0$) and away-side ($|\Delta\phi - \pi| < 1.0$) distributions for ^{3}He + Au, d + Au, and p + Au indicate a sizable impact from nonflow correlations that can be removed with three subtraction methods (termed I, II, III) that utilize the correlation functions from MB p + p as outlined below. Note the similarity between the away-side distributions for ^{3}He + Au, d + Au, p + Au, and that for p + p, which is dominated by nonflow.
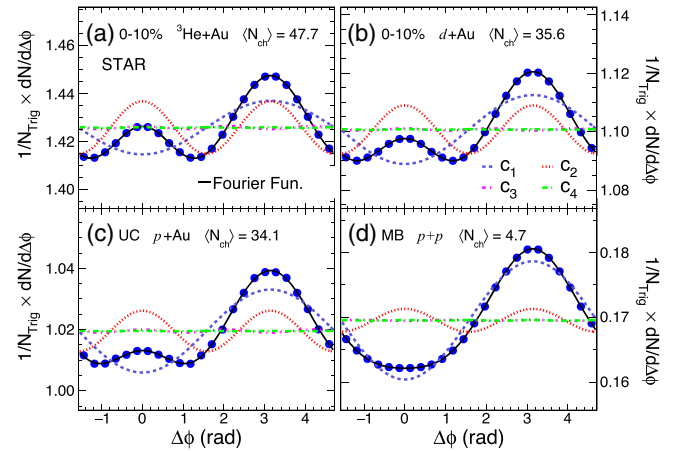
FIG. 1. Two-particle per-trigger yield distributions for ^{3}He + Au, d + Au, p + Au, and p + p collisions at $\sqrt{s_{NN}} = 200$ GeV as indicated. The trigger and associated particles are selected in the range $0.2 < p_T < 2.0$ GeV/c and $1.0 < |\Delta\eta| < 1.8$. An illustration of the Fourier functions fitting procedure to estimate the nonflow contributions and extract the $v_{2,3}$ is also shown.

In all methods, a Fourier function fit of the measured $Y(\Delta\phi)$ distributions is employed to extract $v_n(p_T^{\mathrm{Trig}})$:

$$Y(\Delta\phi, p_T^{\mathrm{Trig}}) = c_0 \left[1 + \sum_{n=1}^{4} 2c_n \cos(n\Delta\phi) \right]. \quad (2)$$

The nonflow contributions are subtracted with

$$c_n^{\mathrm{sub}} = c_n - c_n^{\mathrm{nonflow}} = c_n - c_n^{pp} \times f \quad (3)$$

where the c_n^{sub} is c_n after nonflow subtraction. The methods differ from each other in how the scale factor f is estimated. The c_n is simply the product of v_n for trigger and associated particles, i.e., $c_n = v_n^{\mathrm{Trig}} \times v_n^{\mathrm{Assoc}}$.

Method I assumes that the nonflow correlations between $p + p$ and $p/d/^3\mathrm{He} + \mathrm{Au}$ are the same. Thus the factor f is equal to the ratio of the integral yield of $Y(\Delta\phi)$ (c_0) due to the multiplicity dilution. Then $f = c_0^{pp}/c_0$. This method is found to be similar to the so-called scalar product method [44,45,61] from testing.

The nonflow contributions in $p + p$ collisions could be different from those in $p/d/^3\mathrm{He} + \mathrm{Au}$ collisions; such differences are corrected in Methods II and III by looking into the near-side yield and away-side shape of the nonflow correlations.

pi twb 0.3wMethod II estimates the nonflow contribution to the near-side yield (Y^N) from the difference between the $Y(\Delta\phi)$ yield measured for $0.2 < |\Delta\eta| < 0.5$ and $1.0 < |\Delta\eta| < 1.8$, as outlined in Refs. [46–48]. Then $f = (Y^N/Y_{pp}^N) \times (c_0^{pp}/c_0)$.

With the $|\Delta\eta| > 1.0$ requirement, the residual nonflow arises primarily from the away-side correlations, which is dominated by the c_1 component. Method III uses c_1 to estimate f directly [49], then $f = c_1/c_1^{pp}$.

Method III is also similar to the template fit method [50] as shown in the Supplemental Material [62].

Since $v_n^{\mathrm{Assoc}} \equiv \sqrt{c_n}$ for trigger and associated particles in the same p_T range, one has $v_n^{\mathrm{Trig}} = c_n/v_n^{\mathrm{Assoc}}$. Similarly, the v_n after nonflow subtraction (v_n^{sub}) is computed as $v_n^{\mathrm{sub,Trig}} = c_n^{\mathrm{sub}}/v_n^{\mathrm{sub,Assoc}}$.

The systematic uncertainties associated with $v_{2,3}(p_T)$ have four main contributions: (i) variation of associated detectors used in track matching, (ii) background tracks, (iii) residual pileup effects, and (iv) uncertainties for nonflow subtraction. (i) A comparison of the results obtained with TOF matching and HFT matching shows a difference in $v_2(v_3)$ of less than 3% (10%) for all three systems. (ii) The track background uncertainty is estimated by varying the cut on the number of TPC space points used for track reconstruction from 15 to 25. The resulting values vary less than 5% (10%) in $v_2(v_3)$. (iii) The impact of residual pileup is estimated by comparing results obtained from data with different beam luminosities, giving a difference of less than 2% (5%) for $v_2(v_3)$ for all three systems. (iv) The uncertainties associated with the nonflow

subtraction is estimated by comparing between subtraction methods and $\Delta\eta$ cuts ($|\Delta\eta| > 0.8$, 1.2, and 1.4), as well as between the same-charge and opposite-charge particle pairs. The results from Method III, which are close to the average of the results from the three methods, are taken as the default, and the differences from the other two methods and variations are taken as the systematic uncertainties. The resulting uncertainty is up to 25% (30%) in $v_2(v_3)$. A study based on the HIJING model [63] (shown in the Supplemental Material [62]) indicates that the uncertainties for nonflow subtraction are within the systematic uncertainties assigned here.

Figure 2 shows a comparison of the v_n values extracted for central $^3\mathrm{He} + \mathrm{Au}$, $d + \mathrm{Au}$, and $p + \mathrm{Au}$ collisions before and after nonflow subtraction. The away-side nonflow correlations give a positive contribution to v_2 and a negative one to v_3. Therefore, the subtraction decreases the magnitude of v_2 as shown in the left panels of Fig. 2, but increases the magnitude of v_3 as shown in the right panels. The comparison also indicates that the respective methods give similar results after subtraction.

Comparisons to the published PHENIX measurements [21,22] indicate that, within the uncertainties, the $v_2(p_T)$ results for all three collision systems and the $v_3(p_T)$ results for $^3\mathrm{He} + \mathrm{Au}$ collisions from both experiments are in reasonable agreement with a maximum difference of $\approx 25\%$. However, the STAR $v_3(p_T)$ measurements for $p + \mathrm{Au}$ and $d + \mathrm{Au}$ collisions are about a factor of 3 larger than those reported by PHENIX. This difference is insensitive to the different centrality definitions employed in the two experiments (see the Supplemental Material [62]). The root cause of this discrepancy is still not fully understood. On the other hand, a recent model study [64] indicates that up to 50% of this $v_3(p_T)$ discrepancy could result from the larger longitudinal decorrelation possible in the PHENIX measurements. However, calculations from this model systematically underpredict the individual STAR and PHENIX $v_3(p_T)$ measurements in $p + \mathrm{Au}$ collisions. The data-model comparison may improve in the future with the inclusion of effects such as nonflow and prehydrodynamic flow effects in the calculations.

We compare our results to two hydrodynamic model calculations—SONIC [33,34] and IP-Glasma + MUSIC [65,66]—in Fig. 3. The pre-existing calculations from SONIC are only available for the 0–5% centrality, but the differences from the centrality mismatch are expected to be around 10%. The SONIC model, which roughly describes the PHENIX measurements [21], employs initial eccentricity from nucleon Glauber without subnucleonic fluctuations (Model a). The SONIC calculations show reasonable agreement with the current measurements for $v_2(p_T)$, but underestimate the $v_3(p_T)$ in $^3\mathrm{He} + \mathrm{Au}$ and significantly underestimate the $v_3(p_T)$ in $d + \mathrm{Au}$ and $p + \mathrm{Au}$ collisions by more than 100%. This underprediction could be due to the much smaller ε_3 values without
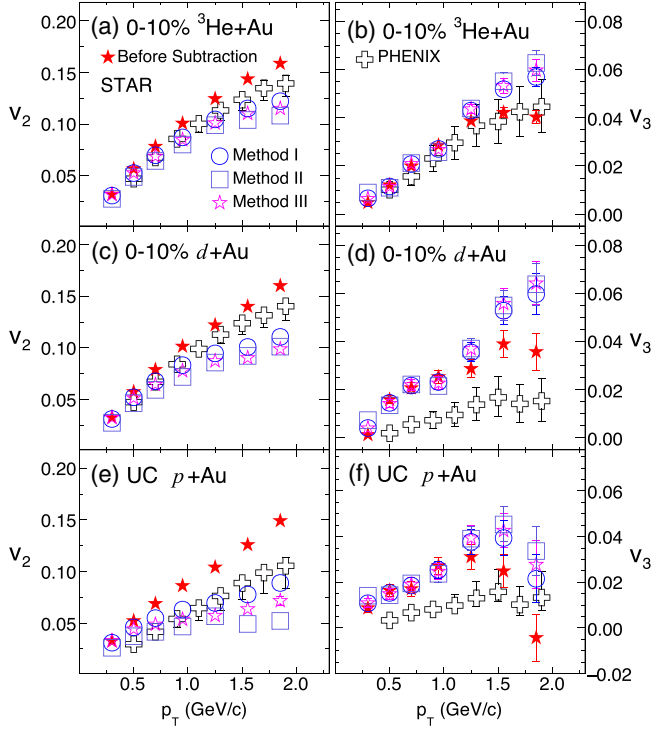
FIG. 2. Comparison of the v_2 (left column) and v_3 (right column) in 0–10% ^{3}He + Au, 0–10% d + Au, and UC p + Au collisions before and after three different nonflow subtraction methods (see text). Only statistical uncertainties are shown. The PHENIX measurements with statistical and systematic uncertainties are also shown.

FIG. 3. Comparison of the $v_{2,3}$ from data and hydrodynamic model calculations in 0–10% ^{3}He + Au, 0–10% d + Au, and UC p + Au collisions. The theory curves are obtained from the SONIC [33,34] and the IP-Glasma + MUSIC [65,66] hydrodynamic models.

subnucleonic fluctuations employed in the calculations. Interestingly, the SONIC calculations give a reasonable prediction of $v_2(p_T)$ for p + Au with the much smaller ε_2 value indicated in Table I. It is currently unclear if this is related to possible uncertainties in the hydrodynamic gradient-expansion corrections or other sources.

The IP-Glasma + MUSIC model includes subnucleonic fluctuations, momentum correlations, and prehydrodynamic flow in the initial state. For the final state, it includes viscous hydrodynamic evolution, and the UrQMD model for evolution in the hadronic phase [65,66]. It is tuned to describe the data for large-sized systems and then extrapolated to small-sized systems without further tuning. In contrast to the SONIC model, the calculations from the IP-Glasma + MUSIC model overpredict the $v_2(p_T)$ data, but show good agreement with the $v_3(p_T)$ data for all three systems. The overprediction could result from (i) an overestimate of the system-dependent ε_2 values employed in the calculations (see Model d in Table I); (ii) the sizable prehydrodynamic flow included in the IP-Glasma + MUSIC model framework.

Figure 3 shows that both models fail to give a simultaneous description of $v_2(p_T)$ and $v_3(p_T)$, indicating that further studies are required to identify model parameters that regulate the influence of the subnucleonic fluctuations
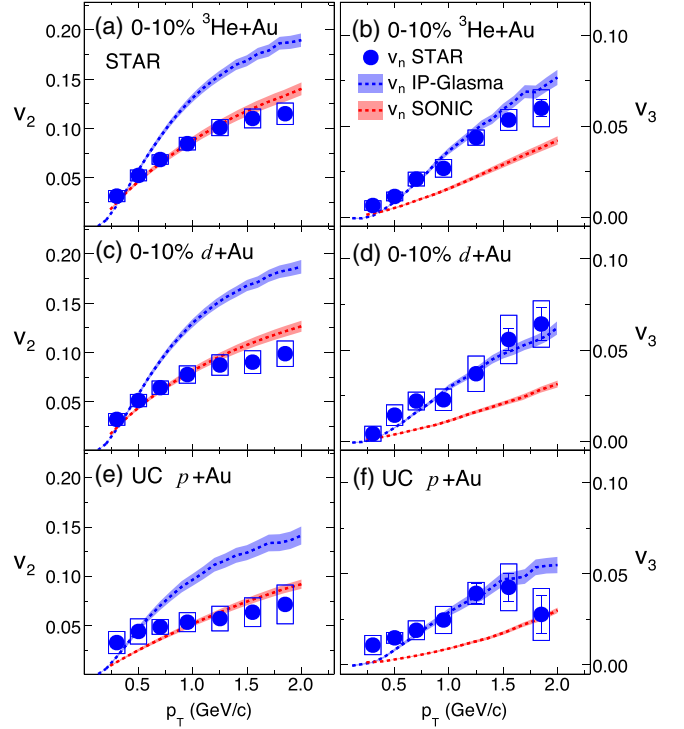
on $\varepsilon_{2,3}$, and a possible influence from longitudinal flow decorrelation [64].

We further compare the difference between these three systems via v_n ratios at similar mean multiplicity $\langle N_{ch} \rangle$, as shown in Fig. 4. Such ratios can give insight into the influence of the initial stage of the collisions since the differences in the final state contributions are expected to be largely canceled for similar multiplicity $\langle N_{ch} \rangle$ [17,67]. We also compare the v_n ratios with the corresponding ε_n ratios in Fig. 4; in the absence of other initial state influences, v_n is expected to be proportional to ε_n. Hence, the comparison of their ratios can serve as a baseline. The ratio $v_{2,pAu}/v_{2,dAu}$ equals to 0.73 ± 0.05 from fitting to a constant. Both systematic and statistical uncertainty are included in the uncertainty. It is close to the ratios of ε_2 for the models with subnucleonic fluctuations ($\varepsilon_{2,pAu}^{b,c,d}/\varepsilon_{2,dAu}^{b,c,d} = 0.65, 0.77$, and 0.68, respectively and only Model c is shown in Fig. 4).

However, it is 6.0σ away from the ratio $\varepsilon_{2,pAu}^a/\varepsilon_{2,dAu}^a = 0.43$ without subnucleonic fluctuations. The ratio $v_{3,^3He+Au}/v_{3,dAu} = 1.00 \pm 0.09$ is also similar to those for ε_3 from the models with subnucleonic fluctuations ($\varepsilon_{3,^3He+Au}^{b,c,d}/\varepsilon_{3,dAu}^{b,c,d} = 1.09, 1.05$, and 1.15, respectively). By contrast, it is 6.2σ away from the $\varepsilon_{3,^3He+Au}^a/\varepsilon_{3,dAu}^a = 1.56$ (without fluctuations). The comparison suggests that

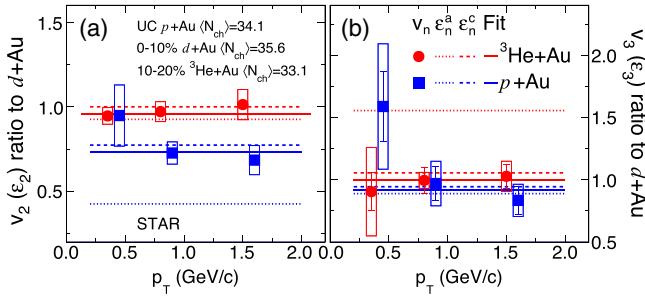FIG. 4. Comparison of the ratios of v_2 (a) and v_3 (b) between a given small system and $d+\mathrm{Au}$ at similar $\langle N_{\mathrm{ch}}\rangle$ for several p_T selections. The solid lines indicate a fit to the data points, and the dashed lines indicate the corresponding eccentricity ratios obtained from Glauber-based model calculations with (ε^c, large dash line) [22,31,32] and without (ε^a, small dash line) [33] subnucleonic fluctuations, respectively.

subnucleonic fluctuations play a crucial role in establishing the initial state geometry. However, these small systems require further model comparisons to their ratios to ascertain a possible influence from other initial stage contributions, such as prehydrodynamics flow.

In summary, we measured $v_{2,3}(p_T)$ in central $^3\mathrm{He}+\mathrm{Au}$, $d+\mathrm{Au}$, and $p+\mathrm{Au}$ collisions at $\sqrt{s_{NN}}=200$ GeV, extracted from two-particle azimuthal angular correlations ($|\Delta\eta|>1.0$) with three subtraction methods designed to mitigate the influence of the nonflow correlations. Results from these methods are consistent within uncertainties. The magnitude of v_2 in $p+\mathrm{Au}$ collisions is lower than that of $d+\mathrm{Au}$ and $^3\mathrm{He}+\mathrm{Au}$ collisions, while the magnitude of v_3 is system independent. The measurements are consistent with a significant influence from subnucleonic eccentricity fluctuations. Hydrodynamic model comparisons to the data suggest that further model constraints, especially for the theoretical parameters which regulate the subnucleonic fluctuations, are required for more detailed characterizations of the azimuthal anisotropy in small-sized systems.

[1] I. Arsene *et al.* (BRAHMS Collaboration), Nucl. Phys. **A757**, 1 (2005).
[2] K. Adcox *et al.* (PHENIX Collaboration), Nucl. Phys. **A757**, 184 (2005).
[3] B. B. Back *et al.* (PHOBOS Collaboration), Nucl. Phys. **A757**, 28 (2005).
[4] J. Adams *et al.* (STAR Collaboration), Nucl. Phys. **A757**, 102 (2005).
[5] G. Roland, K. Safarik, and P. Steinberg, Prog. Part. Nucl. Phys. **77**, 70 (2014).
[6] S. Voloshin and Y. Zhang, Z. Phys. C **70**, 665 (1996).
[7] A. M. Poskanzer and S. A. Voloshin, Phys. Rev. C **58**, 1671 (1998).
[8] Z. Qiu and U. W. Heinz, Phys. Rev. C **84**, 024911 (2011).
[9] R. A. Lacey, Nucl. Phys. **A774**, 199 (2006).
[10] H. Song, S. A. Bass, U. Heinz, T. Hirano, and C. Shen, Phys. Rev. Lett. **106**, 192301 (2011); **109**, 139904(E) (2012).
[11] H. Niemi, G. S. Denicol, H. Holopainen, and P. Huovinen, Phys. Rev. C **87**, 054901 (2013).
[12] F. G. Gardim, J. Noronha-Hostler, M. Luzum, and F. Grassi, Phys. Rev. C **91**, 034902 (2015).
[13] J. Fu, Phys. Rev. C **92**, 024904 (2015).
[14] H. Holopainen, H. Niemi, and K. J. Eskola, Phys. Rev. C **83**, 034901 (2011).
[15] G.-Y. Qin, H. Petersen, S. A. Bass, and B. Muller, Phys. Rev. C **82**, 064903 (2010).
[16] C. Gale, S. Jeon, B. Schenke, P. Tribedy, and R. Venugopalan, Phys. Rev. Lett. **110**, 012302 (2013).
[17] P. Liu and R. A. Lacey, Phys. Rev. C **98**, 021902(R) (2018).
[18] B. Schenke, S. Jeon, and C. Gale, Phys. Lett. B **702**, 59 (2011).
[19] A. Adare *et al.* (PHENIX Collaboration), Phys. Rev. Lett. **114**, 192301 (2015).
[20] A. Adare *et al.* (PHENIX Collaboration), Phys. Rev. Lett. **115**, 142301 (2015).
[21] C. Aidala *et al.* (PHENIX Collaboration), Nat. Phys. **15**, 214 (2019).
[22] U. A. Acharya *et al.* (PHENIX Collaboration), Phys. Rev. C **105**, 024901 (2022).
[23] U. A. Acharya *et al.* (PHENIX Collaboration), Phys. Rev. C **107**, 024907 (2023).
[24] L. Adamczyk *et al.* (STAR Collaboration), Phys. Lett. B **747**, 265 (2015).
[25] J. Adam *et al.* (STAR Collaboration), Phys. Rev. Lett. **122**, 172301 (2019).
[26] S. Chatrchyan *et al.* (CMS Collaboration), Phys. Lett. B **724**, 213 (2013).
[27] B. Abelev *et al.* (ALICE Collaboration), Phys. Lett. B **719**, 29 (2013).

[28] G. Aad *et al.* (ATLAS Collaboration), Phys. Rev. Lett. **110,** 182302 (2013).

[29] M. Aaboud *et al.* (ATLAS Collaboration), Eur. Phys. J. C **77,** 428 (2017).

[30] P. M. Chesler, J. High Energy Phys. 03 (2016) 146.

[31] K. Welsh, J. Singer, and U. W. Heinz, Phys. Rev. C **94,** 024919 (2016).

[32] B. Schenke, P. Tribedy, and R. Venugopalan, Phys. Rev. Lett. **108,** 252301 (2012).

[33] J. L. Nagle, A. Adare, S. Beckman, T. Koblesky, J. Orjuela Koop, D. McGlinchey, P. Romatschke, J. Carlson, J. E. Lynn, and M. McCumber, Phys. Rev. Lett. **113,** 112301 (2014).

[34] P. Romatschke, Eur. Phys. J. C **75,** 305 (2015).

[35] A. Bzdak and G.-L. Ma, Phys. Rev. Lett. **113,** 252301 (2014).

[36] Y. Zhou, X. Zhu, P. Li, and H. Song, Phys. Rev. C **91,** 064908 (2015).

[37] P. Romatschke, Eur. Phys. J. C **75,** 429 (2015).

[38] C. Bierlich, G. Gustafson, and L. Lönnblad, Phys. Lett. B **779,** 58 (2018).

[39] M. Mace, V. V. Skokov, P. Tribedy, and R. Venugopalan, Phys. Rev. Lett. **121,** 052301 (2018); **123,** 039901(E) (2019).

[40] K. Dusling and R. Venugopalan, Phys. Rev. D **87,** 094034 (2013).

[41] M. Nie, L. Yi, X. Luo, G. Ma, and J. Jia, Phys. Rev. C **100,** 064905 (2019).

[42] G. S. Denicol, H. Niemi, E. Molnar, and D. H. Rischke, Phys. Rev. D **85,** 114047 (2012); **91,** 039902(E) (2015).

[43] W. Florkowski, R. Ryblewski, and M. Spaliński, Phys. Rev. D **94,** 114025 (2016).

[44] J. Adams *et al.* (STAR Collaboration), Phys. Rev. Lett. **93,** 252301 (2004).

[45] J. Adams *et al.* (STAR Collaboration), Phys. Rev. C **72,** 014904 (2005).

[46] V. Khachatryan *et al.* (CMS Collaboration), Phys. Lett. B **765,** 193 (2017).

[47] L. Adamczyk *et al.* (STAR Collaboration), Phys. Lett. B **743,** 333 (2015).

[48] G. Aad *et al.* (ATLAS Collaboration), Phys. Rev. C **90,** 044906 (2014).

[49] A. Adare *et al.* (PHENIX Collaboration), Phys. Rev. C **98,** 014912 (2018).

[50] G. Aad *et al.* (ATLAS Collaboration), Phys. Rev. Lett. **116,** 172301 (2016).

[51] W. J. Llope *et al.*, Nucl. Instrum. Methods Phys. Res., Sect. A **759,** 23 (2014).

[52] F. S. Bieser *et al.*, Nucl. Instrum. Methods Phys. Res., Sect. A **499,** 766 (2003).

[53] C. Adler, A. Denisov, E. Garcia, M. Murray, H. Strobele, and S. White, Nucl. Instrum. Methods Phys. Res., Sect. A **499,** 433 (2003).

[54] W. J. Llope (STAR Collaboration), Nucl. Instrum. Methods Phys. Res., Sect. A **661,** S110 (2012).

[55] L. Adamczyk *et al.* (STAR Collaboration), Phys. Rev. C **86,** 054908 (2012).

[56] C. Loizides, J. Nagle, and P. Steinberg, SoftwareX **1–2,** 13 (2015).

[57] S. Agostinelli *et al.*, Nucl. Instrum. Methods Phys. Res., Sect. A **506,** 250 (2003).

[58] V. Fine, Y. Fisyak, V. Perevoztchikov, and T. Wenaus, Comput. Phys. Commun. **140,** 76 (2001).

[59] M. Anderson *et al.*, Nucl. Instrum. Methods Phys. Res., Sect. A **499,** 659 (2003).

[60] M. Szelezniak (STAR Collaboration), *Proc. Sci.*, Vertex2014 (2015) 015.

[61] N. Borghini, P. M. Dinh, and J.-Y. Ollitrault, Phys. Rev. C **64,** 054901 (2001).

[62] See Supplemental Material at http://link.aps.org/supplemental/10.1103/PhysRevLett.130.242301 for the detail study about HIJING simulation, centrality selection and template fit.

[63] M. Gyulassy and X.-N. Wang, Comput. Phys. Commun. **83,** 307 (1994).

[64] W. Zhao, S. Ryu, C. Shen, and B. Schenke, Phys. Rev. C **107,** 014904 (2023).

[65] B. Schenke, C. Shen, and P. Tribedy, Phys. Lett. B **803,** 135322 (2020).

[66] B. Schenke, C. Shen, and P. Tribedy, Phys. Rev. C **102,** 044905 (2020).

[67] P. Liu and R. A. Lacey, Phys. Rev. C **98,** 031901 (2018).